A New Current Source Inverter with Simultaneous Recovery and Commutation

GYU-HYEONG CHO, MEMBER, IEEE, AND SUN-SOON PARK, MEMBER, IEEE

Abstract—**A new current source inverter which is believed to be more advantageous than the autosequentially commutated inverter is proposed. The new current source inverter operates in a much wider frequency range with much lower voltage stress on the motor terminals and power devices. Simulation results show that the new current source inverter is about four times superior to the autosequentially commutated inverter in operating frequency range and in voltage stress. The experimental results are shown for a 5-hp induction motor.**

Introduction

CURRENT source inverters (CSI) are well-known for ac motor drives. The most widely used CSI would be the autosequentially commutated inverter (ASCI) shown in Fig. 1. The ASCI has many advantages such as ruggedness, fuseless protection, full four-quadrant operation, etc. However, ASCI also has quite a few shortcomings, such as

1) large high-voltage capacitors,
2) high-voltage thyristors and power diodes,
3) high-voltage motor terminal stresses,
4) limited range of operating frequency, etc.

Thus the ASCI is usually designed by compromising high-voltage stresses and operating range. In spite of such limitations, the ASCI has been preferred simply because there were no other CSIs comparable to the ASCI.

In this paper a new CSI which is believed to be much more advantageous than the ASCI is proposed. The new CSI, which is called the simultaneous recovery and commutation inverter (SRCI), operates in a much wider frequency range with much lower voltage stress on the motor terminals and the power devices. The SRCI has smoother current waveforms, and furthermore it can be built with considerably lower cost than the ASCI.

Limitations of ASCI with Voltage Clamping

The disadvantages of the ASCI can be overcome partially by slightly modifying the power circuit [1]–[6]. An example is illustrated in Fig. 2, where a voltage clamping circuit (VCC) and an energy recovery circuit (ERC) are shown. By the role of the VCC, a wider range of operating frequency with considerably lowered voltage stresses can be achieved. However, a bulky and expensive ERC is required to recover the clamping energy.

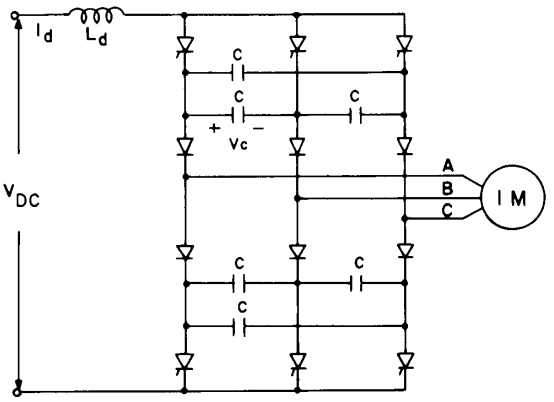

Fig. 1. ASCI inverter.

The bulkiness of the ERC is due partly to the isolation transformer. If the isolation transformer is eliminated and directly connected to the ac input lines, circulating currents exist between upper (lower) groups of inverter and converter thyristors. The circulating current becomes large and distorts the load current waveform severely as the operating frequency rises because the back electromotive force (EMF) of the motor whose rectified value appears in series with the circulating loop increases.

To eliminate the isolation transformer, a dissipation circuit is sometimes used instead of the ERC for the purpose of protecting the high-voltage spikes during commutation intervals. However, the limiting operation should be temporary for a finite short period of overloading; otherwise the inverter efficiency would be lowered seriously, and thus the clamping level of the spike voltages should be set to a high value. In fact, this is not much different from the conventional ASCI.

Improved Method of Reactive Energy Recovery

If the clamping energy is not recovered to the ac input lines but to the motor itself, the circulating current does not exist and the isolation transformer is no longer necessary. In fact, the energy recovery action to the motor itself also occurs in the ASCI. During the commutation interval, the capacitors act to facilitate the recovery and absorption of reactive energy. The fact that the ASCI requires no other kind of ERC is a great advantage; however, such a kind of operation also brings forth the limitations of ASCIs as described previously.

Paper IPCSD 88-12, approved by the Static Power Converter Committee of the IEEE Industry Applications Society for presentation at the 1987 Industry Applications Society Annual Meeting, Atlanta, GA, October 16-23. Manuscript released for publication May 13, 1988.

The authors are with the Electrical Engineering Department, Korea Advanced Institute of Science and Technology, P.O. Box 150, Cheongryang, Seoul, Korea 130-650.

IEEE Log Number 8823821.

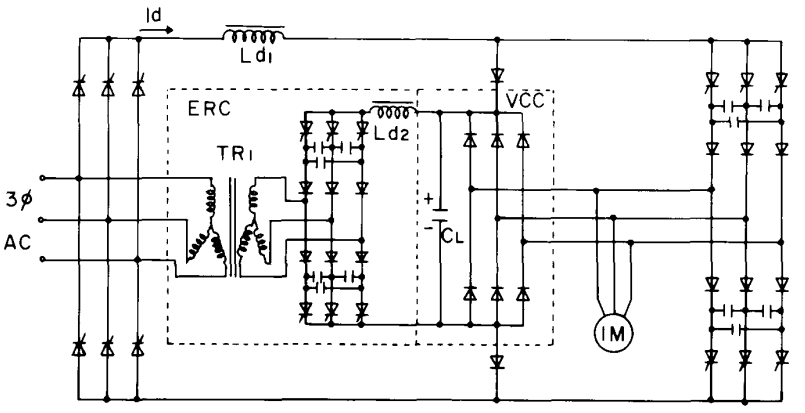

Fig. 2. Voltage-clamped ASCI inverter.

The main reason for the limitations of the ASCI is believed to originate from an inefficiency in utilizing the precharged capacitor energy. Considering the commutating operation of the ASCI, we know that the recovery and absorption operations occur separately and consecutively on the first and second parts of the commutation interval. On the first part, the capacitors simply discharge and recover the energy through the motor windings. On the second part, the capacitors fully absorb the reactive energy of the leakage inductances of the motor, and the final capacitor voltage [7]–[8] becomes

$$V_{co} = E + I_d\sqrt{2L_e/1.5C} \tag{1}$$

where

E line-to-line back EMF at the instant of commutation
L_e per-phase leakage inductance of the motor.

Examining the commutating operation of ASCI more closely, we could find a better way to utilize the recovery energy further. That is, if the recovery energy is exploited to increase (decrease) the next (present) phase current of the motor instead of such simple discharging, the initial current of the absorption interval can be reduced to as low as up to one-half ($I_d/2$). Considering that the capacitor voltage is largely determined by the second term of (1) for heavy-load operation, the peak voltage stresses can also be reduced to about one-half for the equivalent value of commutating capacitance compared with the ASCI. If the capacitance can be increased to be large enough, with low cost and without sacrificing operation bandwidth, then the peak voltage stresses can be controlled by merely adjusting the recovery interval in relation to the load current. The inverter employing such an idea is called the simultaneous recovery and commutation inverter because the capacitor energy recovery and the line-to-line current commutation of the motor start simultaneously.

New GTO SRCI

The SRCI can be realized in several ways. Two SRCI circuits are illustrated in Fig. 3. The power circuit of the SRCI is composed of two inverters, the main inverter and the auxiliary inverter, whose outputs are connected in parallel to the induction motor. The main inverter should have self-commutation capability; however, the auxiliary inverter does not need it. Thus, for the main inverter, thyristors like the ASCI are used in Fig. 3 (a) and GTOs are used in Fig. 3 (b). On the other hand, for the auxiliary inverter, thyristors are simply used. The basic operation principles of the two inverters are the same. Between them, the GTO SRCI is chosen in this paper because of its simplicity to show the proposed idea clearly.

The power circuit of the GTO SRCI looks very different from that of the ASCI in appearance; however, the capacitance C_r of the SRCI corresponds to C of the ASCI in the sense of recovery and of abosorbing the reactive energy. From (1), and considering that the capacitor C_r of the SRCI can be large with small size because it is a dc capacitor, the peak voltage stresses of the SRCI can be reduced considerably; furthermore, if combined with the idea of simultaneous recovery and commutation, the reduction is significant. In fact, the capacitor C_r acts like a spike clamper, and the clamping voltage value can be chosen with great freedom. Of course, for higher frequency operation, the clamping voltage becomes higher; however, the voltage increment is far less severe as compared with the ASCI, which will be shown later.

Operation of the New SRCI

Operation modes of the new SRCI are shown in Fig. 4, starting with a state where GTOs G_{11} and G_{12} are conducting. Typical voltage and current waveforms during the commutation operation from G_{11} to G_{13} are shown in Fig. 5 in which the intervals correspond to respective topology modes. The descriptions of the commutation modes are given below.

From the state of G_{11} and G_{12} conducting (interval I), the commutation (interval II) starts with thyristors T_{23} and T_{24} of the auxiliary inverter turned on. The positive-side dc link current flowing through G_{11} begins to split from terminal A to terminal B of the motor by the voltage across the capacitor C_r. Therefore the capacitor discharges, thus recovering its energy through the motor windings.

During this interval, the currents of phases A and B and the capacitor voltage are given by

$$i_b = (V_r/Z_e)\sin(\omega_d t) \tag{2}$$

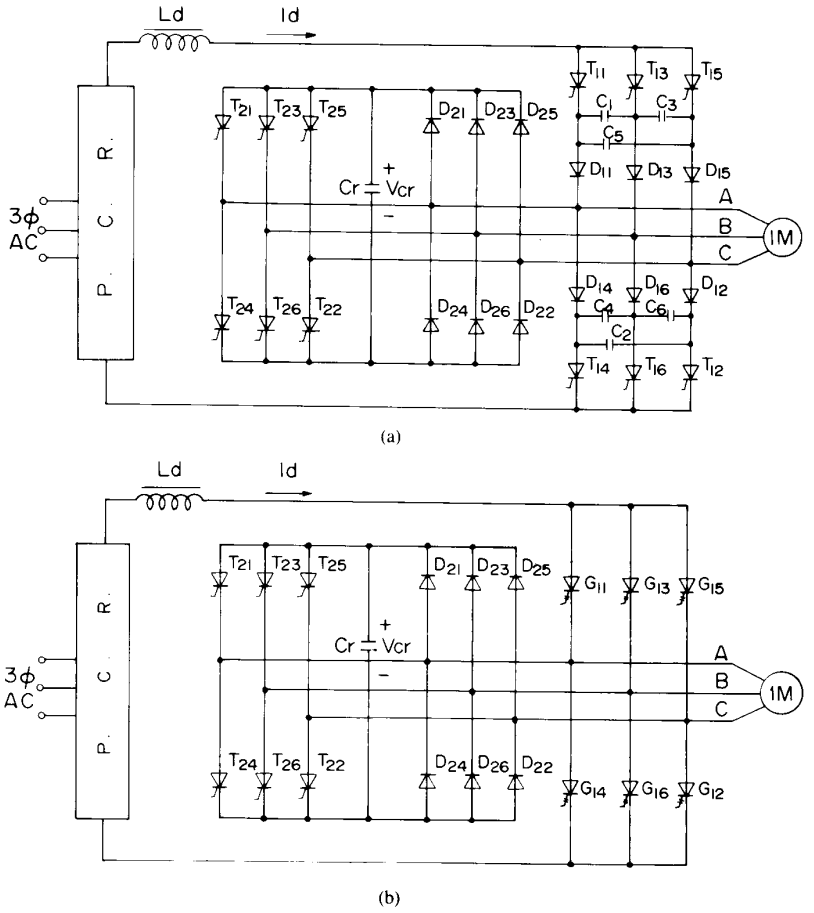

Fig. 3. New SRCI inverters. (a) Thyristor SRCI. (b) GTO SRCI.

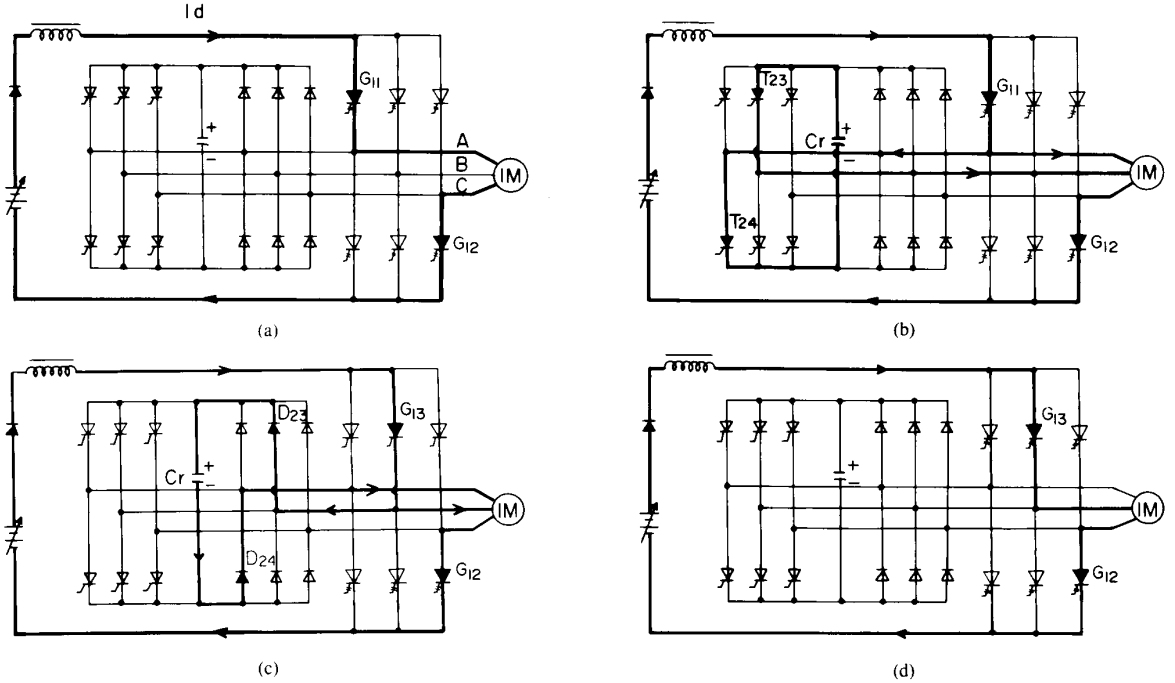

Fig. 4. Operation modes of SRCI inverter. (a) Mode I. (b) Mode II. (c) Mode III. (d) Mode IV.

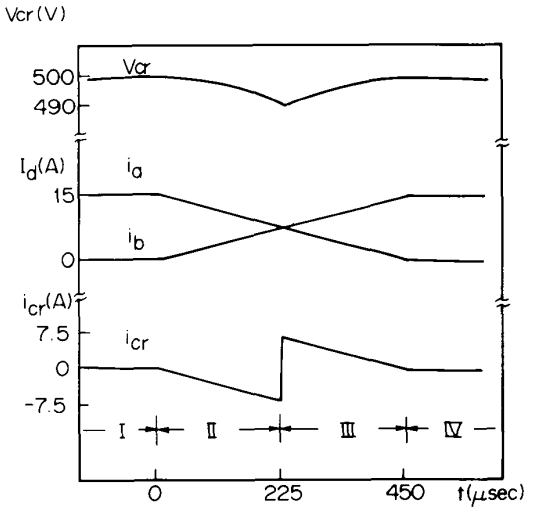

Fig. 5. Waveforms during commutation interval of SRCI.

$$i_a = I_d - i_b \tag{3}$$

$$V_{cr} = V_{co} - V_r(1 - \cos(\omega_d t)) \tag{4}$$

where

$$V_{co} = V_{cr}(0)$$

$$E_1 = \frac{1}{\tau_r}\int_0^{\tau_r} e_{ab}\, dt$$

$$V_r = V_{co} + E_1$$

$$Z_e = \sqrt{2L_e/C_r}$$

$$\omega_d = 1/\sqrt{2L_eC_r}.$$

After a finite period of time, τ_r, interval III starts by turning on G_{13} and turning off G_{11}. The auxiliary thyristors T_{23} and T_{24} are automatically turned off at the beginning of this interval because the current path is changed and formed through the diodes D_{23} and D_{24}. In this case, note that the current direction of the capacitor C_r is also changed. This is the charging interval; in other words, absorbing interval at C_r from the leakage inductance energy of the motor.

During this interval, the currents of phase A and B and the capacitor voltage are given by

$$i_b = (V_r/Z_e)\sin(\omega_d t) + I_d(1 - \cos(\omega_d(t - \tau_r))) + (\Delta E/Z_e)\sin(\omega_d(t - \tau_r)) \tag{5}$$

$$i_a = I_d - i_b \tag{6}$$

$$V_{cr} = V_{co} - V_r(1 - \cos(\omega_d t)) + Z_e I_d \sin(\omega_d(t - \tau_r)) + \Delta E(1 - \cos(\omega_d(t - \tau_r))) \tag{7}$$

where

$$\Delta E = E_1 - E_2$$

$$E_2 = \frac{1}{\tau_r}\int_{\tau_r}^{2\tau_r} e_{ab}\, dt.$$

Interval IV starts with G_{13} and G_{12} conducting when all of the energy stored in the leakage inductance finishes discharging.

From the operations described in the preceding, we know that the energy recovery of C_r and the terminal current commutation of the motor start simultaneously in interval II, and the amount of recovery energy seems to be proportional to the interval length. However, the amount of recovery energy does not depend on τ_r except during the load transient. In other words, when the steady state is reached, the amount of recovery energy of C_r becomes constant if the load is constant, and the B terminal current reaches about one-half of the dc link current with the same amount of reduction in A terminal current. Thus constant energy recovery occurs whether the interval time τ_r is long or short. Furthermore, the duration of interval III becomes nearly equal to the length of interval II during the steady-state operation.

The control of τ_r is closely related to the maximum operating frequency of the inverter. Since τ_r can be determined almost arbitrarily, the maximum operating frequency can also be arbitrarily determined. However, it should be pointed out that the capacitor voltage in the steady state varies as a function of τ_r and load current. As τ_r reduces more and the load current increases more, the capacitor voltage rises higher; however, the rate of increment is far less severe compared with ASCI because the A terminal current is reduced to one-half at the start of the charging interval, and the capacitance (C_r) can have a large value with small size and low cost.

Since the capacitance (C_r) can be large, the voltage across C_r remains almost constant and the ripple is low during the commutation interval. Thus C_r acts like a voltage source and clamps the spikes of the terminal voltage waveforms of the motor. Therefore the peak voltage stresses of the switching devices and the motor terminals are all limited to the voltage across the capacitor, which is another advantage of the SRCI. Line-to-line voltage, line current, and capacitor current waveforms are illustrated in Fig. 6.

Steady-State Operation

It is interesting to see the operation of the SRCI in the steady state. The final capacitor voltage should be equal to the initial value of (4) when the steady state is reached; that is,

$$V_{cr}|\,t_c = V_{co}. \tag{8}$$

Also the final value of the current of phase B when $t = t_c$ is

$$i_b|\,t_c = I_d. \tag{9}$$

From (5), (7), (8), and (9) we obtain a relation as

$$t_c \cong 2\tau_r. \tag{10}$$

Equation (10) means that the recovery interval (mode II) is almost equal to the absorption interval (mode III) in the steady state. Capacitor voltage stress V_{co} can also be calculated approximately as

$$V_{co} \cong -E_1 + (I_d/2)\sqrt{2L_e/C_r}\sin(\omega_d\tau_r). \tag{11}$$

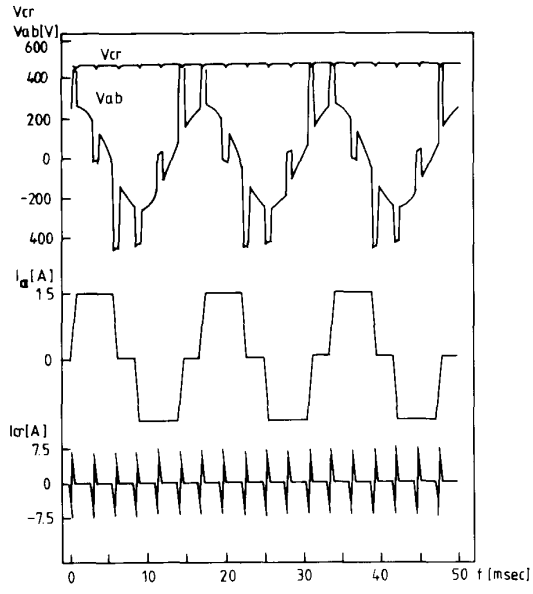

Fig. 6. Waveforms of steady-state operation of SRCI.

Comparing (11) with (1), we know that the voltage stress of the SRCI increases as τ_r reduces; however, it can be lowered significantly (as compared with the ASCI) by properly increasing C_r and τ_r values. If C_r increases enough, $\omega_d \tau_r$ becomes smaller for a lower range of τ_r—say $\tau_r < 1$ ms—then (11) can be approximated as

$$V_{co} \cong -E_1 + L_e I_d / \tau_r. \tag{12}$$

Equation (12) shows that the capacitor voltage becomes proportional to I_d and inversely proportional to τ_r. Alternatively, V_{co} can be set to a constant value almost independent of I_d by controlling τ_r proportional to I_d when C_r is increased to be sufficiently large, in which case note that V_{co} is no longer a function of C_r.

For a large value of C_r, the capacitor actually behaves like a voltage clamper; however, the voltage ripple, ΔV_{cr}, during the commutation interval depends on the capacitance value. The ripple voltage magnitude can be approximated from (4) and (11) as

$$\Delta V_{cr} \cong (L_e / 4V_r)(I_d^2 / C_r). \tag{13}$$

For most cases, however, C_r can be chosen so that ΔV_{cr} becomes small and negligible, compared to V_{co}, for the maximum dc-link current I_d.

One more thing we could know from (11) and (2) is that

$$I_{b1} \cong I_d / 2. \tag{14}$$

Equation (14) is obtained independent of τ_r, which means the recovery energy of the capacitor is equal to nearly half of the stored energy of the motor leakage inductance whether τ_r is short or long. In other words, the recovery energy and the absorption energy of the capacitor is balanced independent of τ_r by a variation of the clamping voltage in the steady state.

Simulation of SRCI Commutation

Computer simulation of the SRCI commutation circuit is performed for a 5-hp induction motor whose data are given:

rated rms line-to-line voltage	$V_r = 220$ V
rated rms line current	$I_r = 15$ A
rated rms magnetizing current	$I_m = 4.5$ A
base frequency	$f_b = 60$ Hz
rated speed	$N_r = 1735$ r/min
per-phase leakage inductance	$L_e = 5.6$ mH.

Fig. 7 shows V_{co} as a function of dc link current I_d for seven values of τ_r from 100 to 700 μs. This figure is obtained for $C_r = 100$ μF, assuming the motor runs with 60-Hz inverter frequency. From the curves we know that the peak capacitor voltage decreases as τ_r increases and increases as I_d increases.

Fig. 8 shows several simulated waveforms of the capacitor voltage during a commutation period when the motor runs with rated load and rated frequency in the steady state. The waveform is shown for a fixed τ_r of 220 μs by varying C_r from 20 to 1000 μF. From the waveforms we see that the ripple magnitude increases with decreasing capacitance and the peak voltage becomes slightly changed for such a large range of C_r values.

Fig. 9 shows the simulated peak capacitor voltage V_{co} during abrupt load transient in between $I_d = 10$ A and 15 A when C_r is fixed and set to 100 μF at 60-Hz operation of the motor. During the load transient shown in Fig. 9, the capacitor voltage changes due to the variation of the interval length of mode III because the interval length of mode II is fixed. Mode III interval becomes longer for the rising transient of load current and becomes shorter for the falling transient, and if the steady state is reached, the interval length again becomes almost equal to τ_r.

Sometimes a problem may occur during the rising transient if the inverter operates near the maximum operating frequency, because the inverter might fail due to the unnecessarily long commutation time in the load transient. Another unfavorable factor during the load transient of Fig. 9 is that the peak voltage stress also varies as a function of I_d, similar to the case of the conventional ASCI. These two problems can be solved by controlled τ_r as a function of I_d. Fig. 10 shows τ_r versus I_d in order to maintain the peak capacitor voltage constant to respective values. In this case, it is assumed that the motor runs at 60 Hz and C_r is chosen to be 100 μF. From the curves we know that it is fairly simple to control τ_r as a function of I_d in order to maintain V_{co} to a constant value greater than 500 V because it is almost a linear function of I_d for the higher range of V_{co}.

Maximum Operating Frequency of the SRCI and Comparison with the ASCI

The limitation of the maximum operating frequency of the conventional ASCI is determined by the no-load condition, because it takes a long time to discharge and charge the commutation capacitors fully and inversely for every commu-

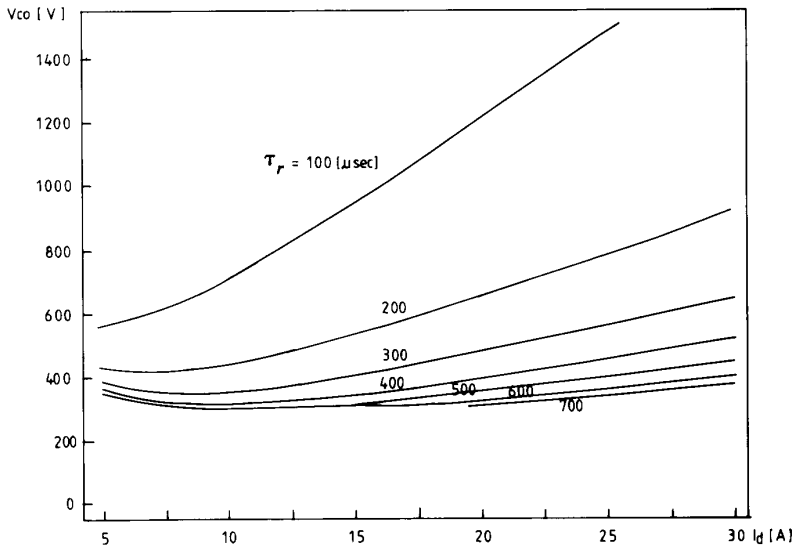

Fig. 7. Capacitor voltage versus dc-link current for several values of τ_r at 60-Hz operation.

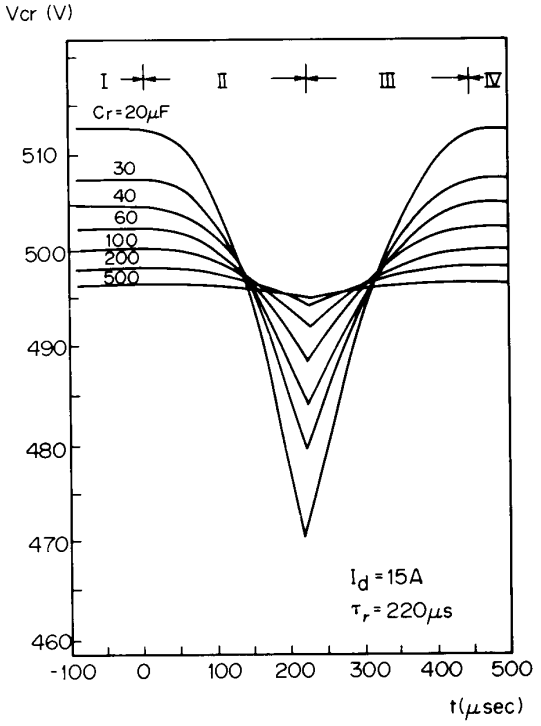

Fig. 8. Capacitor voltage waveforms during commutation interval.

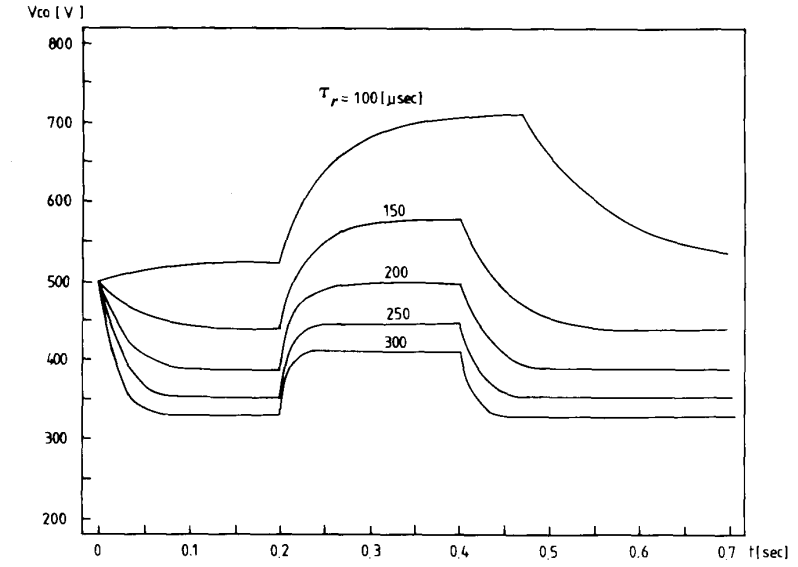

Fig. 9. Capacitor voltage waveforms during abrupt load current transient in between 10 and 15 A.

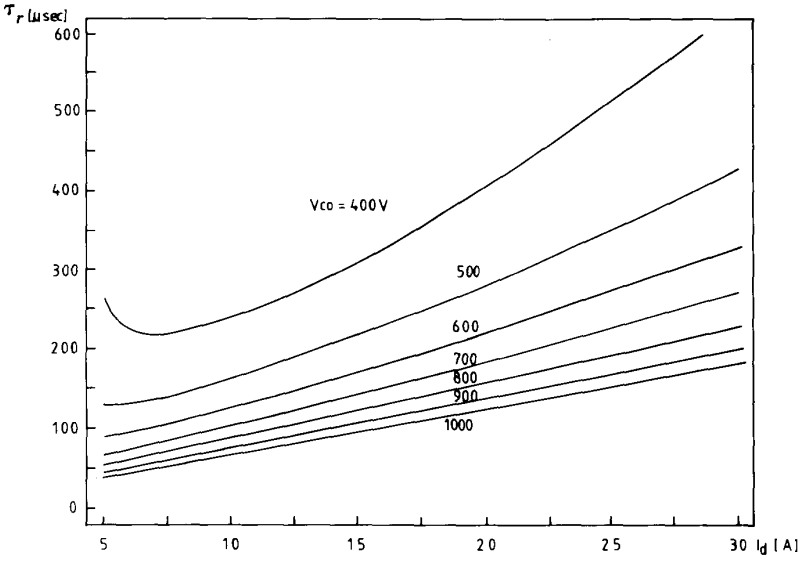

Fig. 10. Recovery interval versus dc link current for several capacitor voltage.

tation. However, the SRCI does not have the maximum frequency limitation at no load but has the limitation at the maximum load due to its unique operating principle. Another difference is that the minimum allowable commutation time of the ASCI is about one-third of the period of the maximum operating frequency at no load. On the other hand, the minimum allowable commutation time of the SRCI is roughly one-sixth of the minimum period at maximum load.

Fig. 11 shows the maximum operating frequencies of the SRCI for above the rated load, up to about 200-percent overload in order to keep the peak capacitor voltage constant to respective values in the range from 400 to 1000 V. In this graph a 100-μF dc capacitor is used for C_r, and τ_r is controlled according to I_d as in Fig. 10.

For a comparison of the methods, Table I and Table II are given [7]–[8]. Table I shows the maximum operating frequencies to limit the peak voltage stresses of the capacitors to three different values of the 100- and 200-percent load conditions, respectively. On the other hand, Table II shows the allowable peak voltage stresses of the capacitor for the three different values of operating frequencies when the load conditions are given by 100 and 200 percent, respectively.

Summarizing the results briefly, it might be good to say that the SRCI is roughly four times superior to the ASCI in the maximum operating frequencies or in the peak voltage stresses. As an example, for a 100-percent load the maximum operating frequency of the ASCI reaches approximately two times the base frequency with about 750-V peak stress; on the

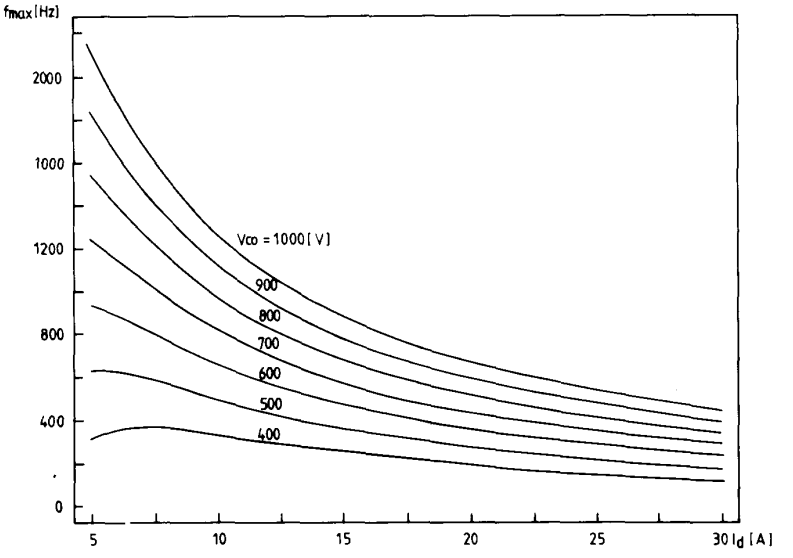

Fig. 11. Maximum operating frequency curves of SRCI.

TABLE I
COMPARISONS AT FIXED VOLTAGE STRESSES

Peak Voltage Stress (V)	Maximum Operating Frequency at 100-Percent Load ($i_d = 15$ A)		Maximum Operating Frequency at 200-Percent Load ($I_d = 30$ A)	
	ASCI (Hz)	SRCI (Hz)	ASCI (Hz)	SRCI (Hz)
500	80	370	0	190
750	135	630	71	327
1000	185	885	97	457

TABLE II
COMPARISONS AT FIXED OPERATING FREQUENCIES

Load	Maximum Operating Frequency (Hz)	Peak Voltage Stress (V)	
		ASCI	SRCI
100 percent ($I_d = 15$ A)	60	400	400
	120	690	400
	240	1270	400
200 percent ($I_d = 30$ A)	60	635	400
	120	1219	400
	240	2385	590

other hand, the SRCI can operate well beyond ten times the base frequency for the corresponding peak voltage stress.

Experimental Results

The experiment of the proposed SRCI was performed for the induction motor of which the parameters were the same as those used for the computer simulation. The capacitor voltage was controlled approximately proportional to the inverter frequency by adjusting the recovery time given by (12), and thereby the peak voltage stresses could be reduced further in the range below the base frequency range. Fig. 12 shows the curves of the experimental results compared with those of theory for τ_r as a function of I_d and inverter frequency to adjust V_{co} to predetermined values, where the maximum voltage is limited to 500 V for linearity of the control characteristic.

The results show fairly good agreement with the simulation results throughout the whole range, although there are some errors in the lower range of I_d caused by the approximations of the back-EMF voltages of the motor. Fig. 13 shows the theoretical and experimental results of the V_{co} kept almost constant in a wide range of I_d, from 5 to 15 A for several values of the inverter frequencies when the recovery interval τ_r is controlled as shown in Fig. 12.

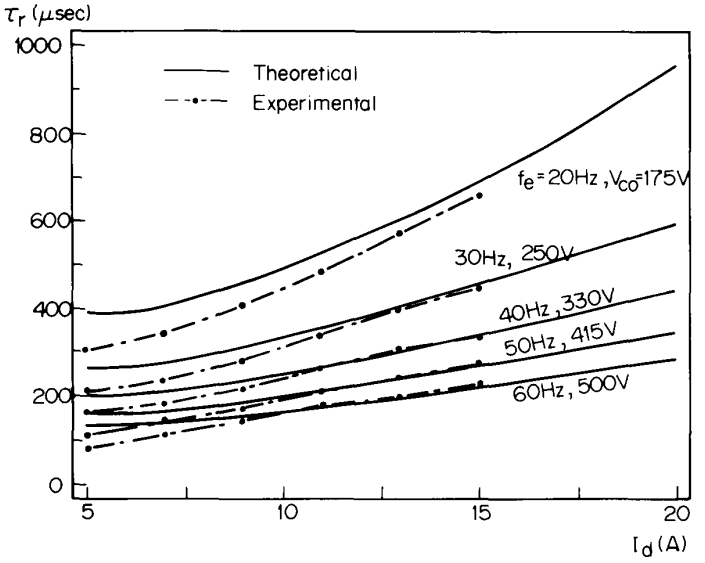

Fig. 12. Comparisons between theoretical and experimental values of τ_r versus I_d for several frequencies.

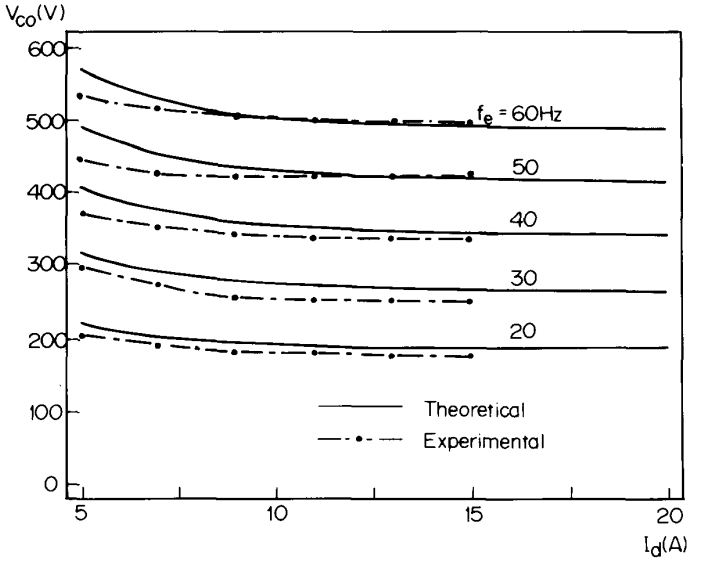

Fig. 13. Variations of V_{co} between theoretical and experimental values for several frequencies.

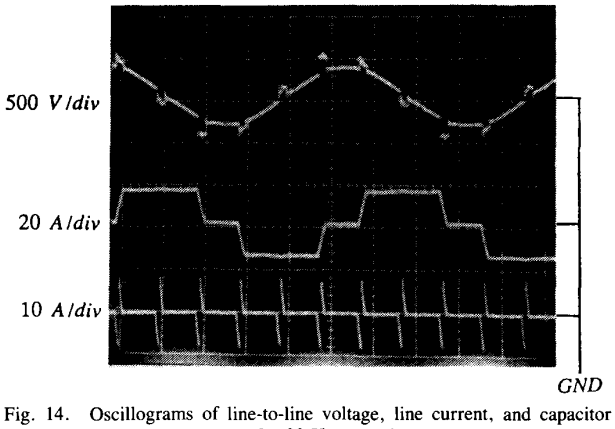

Fig. 14. Oscillograms of line-to-line voltage, line current, and capacitor current for 90-Hz operation.

Fig. 14 shows the oscillograms of line-to-line voltage, line current, and capacitor current, respectively, when the inverter operates at 90 Hz with I_d = 15 A, where the peak spike voltage is shown to be clamped to 500 V, which is equal to V_{co}. In this figure the peak spike voltage is clamped to the same value as in the case of 60 Hz because the inverter operates in the field-weakening range by making the back-EMF voltage constant above 60 Hz.

Fig. 15 shows the details of the commutation interval waveforms, V_{cr}, line current, and capacitor current, respectively, when the inverter operates at 90 Hz. The differences of the waveforms between the experimental and simulation results are due to the snubber circuits of the auxiliary thyristors and the equivalent series resistance of the capacitor, however, which has little influence on the system operation when properly designed.

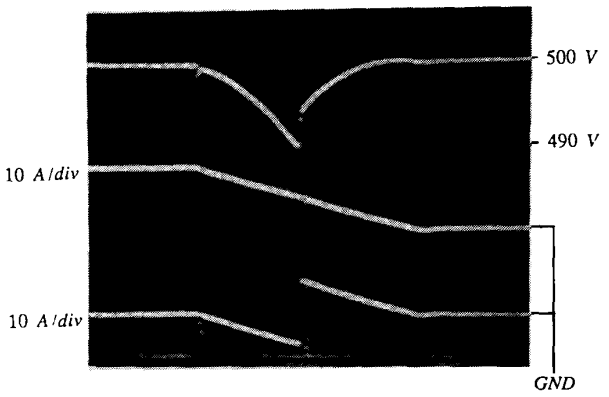

Fig. 15. Oscillograms of capacitor voltage (top), line current (middle), and capacitor current (bottom) during commutation interval for 90-Hz operation; 100 μs/div.

Conclusion

A new SRCI is proposed, and the operating features are proved through experiment. The distinctive merits of the SRCI are low voltage stress on the devices and the motor terminals, a higher operating frequency range, and good reliability. The SRCI requires only a small-size dc capacitor, and thus the system cost is estimated to be considerably low. Since all of the commutation energy is returned to the load, the overall efficiency is also high. We think that the SRCI is an excellent candidate for future drive applications because of its numerous merits.

References

[1] K. P. Phillips, "Current source converter for ac motor drives," *IEEE Trans. Ind. Appl.*, vol. IA-6, no. 6, pp. 679–683, Nov./Dec. 1972.

[2] W. Farrer and J. D. Miskin, "Quasi-sinewave fully regenerative inverter," *Proc. Inst. Elec. Eng.*, vol. 120, pp. 969–976, Sept. 1973.

[3] S. Martinez and F. Aldana, "Current-source double dc-side forced commutation inverter," *IEEE Trans. Ind. Appl.*, vol. IA-14, no. 6, Nov./Dec. 1978.

[4] G. H. Cho and S. B. Park, "Novel six-step and twelve-step current source inverters with dc-side commutation and energy rebound," *IEEE Trans. Ind. Appl.*, vol. IA-17, no. 5, pp. 524–532, Sept./Oct. 1981.

[5] R. H. Osman, "A simple energy-absorbing circuit for current-source inverter," *IEEE Trans. Ind. Appl.*, vol. IA-20, no. 6, Nov./Dec. 1984.

[6] R. G. Palaniappan, "Voltage clamping circuits for CSI/IM drives," *IEEE Trans. Ind. Appl.*, vol. IA-21, no. 2, Mar./Apr. 1985.

[7] R. H. Nelson and T. A. Radomski, "Design methods for current source inverter/induction motor drive systems," *IEEE Trans. Ind. Electron. Contr. Instrum.*, vol. IECI-22, no. 2, May 1975.

[8] M. Showleh, W. A. Maslowski, and V. Stefanovic, "An exact modeling and design of current source inverter," in *Conf. Rec. 1979 IEEE-IAS Ann. Meeting*, pp. 439–459.

Gyu H. Cho (S'76–S'78–M'80) was born in Korea on April 19, 1953. He received the M.S. and Ph.D. degrees from Korea Advanced Institute of Science and Technology (KAIST), Seoul, Korea, in 1977 and 1981, respectively.

From 1982 to 1983 he was with the Electronic Technology Division of the Westinghouse R&D Center, Pittsburgh, PA, where he worked on unrestricted frequency changer systems and inverters. Since 1984 he has been an Assistant/Associate Professor of the Electrical Engineering Department of KAIST. His research interests are in the area of static power converters and drives, resonant converters, and integrated linear electronic-circuit design.

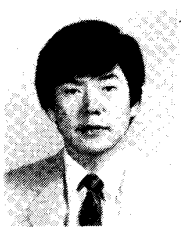

Sun S. Park (S'82–M'84) was born in Korea in 1961. He received the B.S. degree in electrical engineering from Han-Yang University, Seoul, Korea, in 1984, and the M.S. degree in electrical engineering from the Korea Advanced Institute of Science and Technology (KAIST), Seoul, Korea, in 1986. He is presently working towards the Ph.D. degree in electrical engineering at KAIST.

His research interests include power converters and inverters, especially on dc and ac drives.